Journal of South American Earth Sciences 105 (2021) 102964

Contents lists available at ScienceDirect

Journal of South American Earth Sciences

journal homepage: www.elsevier.com/locate/jsames

New thermocronological data of the Cretaceous-Cenozoic clastic sequences from the VINCHINA basin: Linkage between burial, exhumation and thermal flow variations

Cecilia Wunderlin [a,*], Gilda Collo [a], Mauricio Parra [b], Miguel Ezpeleta [a], Francisco Sánchez Nassif [a], Marlene Flores [b], Edward R. Sobel [c], Johannes Glodny [d]

[a] Consejo Nacional de Investigaciones Científicas y Tecnológicas (CONICET), Centro de Investigaciones en Ciencias de la Tierra (CICTERRA), Av. Vélez Sarsfield 1611, X5016CGA, Córdoba, Argentina
[b] Institute of Energy and Environment (IEE), University of Sao Paulo, 05508-010, São Paulo, Brazil
[c] Institut für Geowissenschaften, Universität Potsdam, Karl-Liebknecht-Str. 24-25, 14476, Potsdam, Germany
[d] GFZ German Research Centre for Geosciences, Telegrafenberg, Building B, 14473, Potsdam, Germany

ARTICLE INFO

Keywords:
AFT
(U–Th)/He
Inverse thermal modeling
Thermal regime
Vinchina basin
Cretaceous-Cenozoic sedimentary basin

ABSTRACT

New apatite fission track (AFT) and (U–Th)/He (AHe) data from two sections recording Cretaceous-Cenozoic clastic successions (La Flecha - La Troya Sur creeks) in the northern sector of the Central Precordillera of Argentina are presented. The results show that the Ciénaga del Río Huaco, Puesto la Flecha and Vallecito Fms. would have crossed the 60 °C isotherm during burial, while the middle sector of the Vinchina Fm. would not have reached temperatures higher than 55 °C. Multimethod inverse thermal modeling suggests that the AFT ages of all the studied levels would not have been completely reset and allow inferring that the partial retention zone for the AHe system (AHe-PRZ) would have been reached during the Miocene in levels between the Vallecito and Vinchina Fms. Our 1D-modeling results for the Ciénaga del Río Huaco, Puesto la Flecha and Vallecito Fms. show that the maximum temperature would have been reached at ~15 Ma, with a sedimentary thickness of ~2750 m and a heat flow of 65 mW/m^2. From these data, a geothermal gradient of ~27 °C/km at this time could be inferred. In turn, the Vinchina and Zapallar Fms. would have reached their maximum temperature at ~2 Ma, under a cooler thermal regime (20 mW/m^2) and with an estimated geothermal gradient of <15 °C/km. Thus, a complex time-temperature trajectory is proposed. Maximum and cooling temperatures reached by each unit do not correspond in all cases to the maximum burial and exhumation times. Comparison of the thermal modelling from this work with those carried out by other authors for sections immediately to the north allows us to infer that the thermal regime within the Vinchina basin has important lateral variations. Finally, AFT and AHe analyzes carried out in this work constitute a baseline database of the thermal regime, which is necessary for future multiproxies studies that are being done to evaluate the preservation of primary thermal signals, and thus check their reliability for pealeoclimatic and paleoenvironmental interpretations.

1. Introduction

Post-depositional thermal histories of sedimentary basins are of broad interest in various geological fields. In this regard, low temperature thermal proxies are used in a wide variety of sedimentary records to make inferences regarding the temperatures associated with preserved paleoclimatic and diagenetic processes. Classic proxies used in this type of studies are analysis of clay minerals, fluid inclusions, organic matter maturity, and isotopic and thermochronological indicators, among others. Although these proxies are applied in many and varied contexts, they are usually used individually (a single analytical method or a single proxy; Thiry and Dupuis, 2000; Birks and Birks, 2006; Fagel, 2007) and to solve specific problems without weighing the influence of the variety of superimposed processes that affect the sedimentary units from their deposition, lithification, to their deep burial. As an example, studies based on associations of clay minerals to establish either paleoclimatic and paleoenvironmental conditions or post-depositional processes could be mentioned. Although some studies of paleoclimatic and

* Corresponding author.
E-mail address: c.wunderlin@unc.edu.ar (C. Wunderlin).

https://doi.org/10.1016/j.jsames.2020.102964
Received 15 June 2020; Received in revised form 24 September 2020; Accepted 14 October 2020
Available online 5 November 2020

paleoenvironmental conditions of different geological periods based on this proxy take into account the influence of diagenetic processes (eg. Daoudi et al., 2010), many others do not consider such influence or subjectively assume that diagenesis can be negligible (e.g., Thiry, 2000; Net et al., 2002; Ruffell et al., 2002; Daoudi et al., 2008; Raucsik and Varga, 2008; Bauluz et al., 2014). Similarly, many studies that attempt to establish paleothermal conditions, geodynamic contexts and geothermal gradients do not take into account possible compositional variations related to paleoenvironmental changes or primary source variations (e.g., Hower et al., 1976; Merriman et al., 1999; Collo et al., 2011; Clauer and Lerman, 2012). For this reason, in order to make inferences regarding the temperatures associated with different processes coexisting during the evolution of a basin, it is necessary to perform detailed studies that allow discriminating the primary signals from those linked to the processes of shallow and deep diagenesis. A first step in this direction is to know the thermal-temporal regime that affected a sedimentary basin during its post-depositional history.

Thermochronological analysis constitute one of the most widely used techniques by the geological community in recent decades for the reconstruction of time-temperature burial histories of sedimentary basins (e.g. Naeser et al., 1989; Armstrong and Chapman, 1998; Armstrong, 2005; Tagami and O'Sullivan, 2005; Ketcham 2012; Mahoney et al., 2019; Pujols et al., 2020). In particular, apatite fission tracks (AFT) and (U–Th)/He in apatites (AHe) have been used to establish thermal histories at temperatures between ~ 60 °C and 110–140 °C, and ~60 °C and 75–80 °C, respectively, intervals known as "partial annealing zone" and "partial retention zone" (PAZ and PRZ; Ketcham et al., 1999; Farley, 2002). These proxies are considered as systems almost exclusively affected by thermal and temporal factors associated with post-depositional processes, which allows us to rule out the influence of factors associated with paleoenvironmental dynamics, such as primary composition and early mineral neoformation. Moreover, the post-depositional thermal history of a sedimentary basin may not be as simple as it is interpreted in most cases from thermochronological studies, i.e. considering a stable thermal regime through time and maximum temperatures and cooling ages related with maximum depths and exhumation stages, respectively. Actually, this history can be much more complex.

In this work, we present thermochronological analysis of two geological sections (La Flecha - La Troya; Fig. 1) within the northern limit of the Argentine Precordillera and the Western Sierras Pampeanas. These sections are located on the eastern flank of the syncline that constitutes the La Flecha range, in La Rioja province, and preserve a thick and relatively continuous Cretaceous-Cenozoic strata. Although several authors have carried out studies characterizing and modeling the evolutionary history of these sections (Ciccioli et al., 2010; Collo et al., 2015), no AFT analyses have been performed. In this region, a transition from normal to flat subduction regime during the Cretaceous-Cenozoic time interval has been interpreted (Kay et al., 1991; Gutscher et al., 2000; Jordan et al., 2001; Kay and Mpodozis, 2002; Ramos et al., 2002; Yañez et al., 2002; Ramos and Folguera, 2009; Gans et al., 2011; Collo et al., 2018) and discrepancies exist regarding the associated thermal regime (see Collo et al., 2011; Stevens Goddard and Carrapa, 2018), both at regional and local scales (Stevens Goddard and Carrapa, 2018). So, it constitutes an ideal scenario to make inferences regarding the effects of a changing thermal regime on the post-depositional history. Specifically, the AFT and AHe carried out in this work allows decipher the temperatures reached after deposition, their relationship with the basin thermal regime and its variations between the Cretaceous and Cenozoic and, consequently, to improve the understanding of the relations between the thermal field and the geodynamics in this region.

Furthermore, as these strata records paleoclimatic, paleoenvironmental (Ciccioli et al., 2005, 2010) and lithological variations, clay minerals, fluid inclusions and isotopic analyses are being carried out. In this context, this study will also constitute a baseline of knowledge of the thermal regime necessary for future evaluation of the preservation of the primary signals of these proxies, and thus define their reliability for future pealeoclimatic and paleoenvironmental interpretations.

2. Geological framework and thermochronological background

The sections studied in this work include the sediments belonging to one of the depocenters associated with the extension that affected the central-western region of Argentina during the Cretaceous (Franzese et al., 2003), and the overlapping synorogenic deposits of the Cenozoic Vinchina foreland basin (eg. Jordan et al., 1993). These Cretaceous-Cenozoic sequences were affected by Andean deformation during the Cenozoic and are exposed in the northern frontal zone of the fold and thrust belt (Allmendinger and Judge, 2014).

The study area is in the northern boundary of the Argentine Precordillera with the Western Sierras Pampeanas (La Rioja province, Fig. 1 a, b), approximately 20 km north-northwest to the town of Guandacol. It forms part of the eastern flank of the La Flecha syncline, which is composed of a relatively continuous Cretaceous-Cenozoic sedimentary succession (Fig. 1c) overlying the Triassic-Jurassic Santo Domingo Fm. (Ciccioli et al., 2005; Tedesco et al., 2007).

The Cretaceous strata correspond to the upper-middle part of Ciénaga de Río Huaco Fm. (Ciccioli et al., 2005; Limarino et al., 2000; Tedesco et al., 2007), which consists of ~120 m thick fluvial and playa lake deposits. This formation lies conformably on the red strata of the Triassic Santo Domingo Fm. and are superseded by Cenozoic units of the Vinchina foreland basin above a paraconcordance surface (Limarino et al., 2001; Ciccioli et al., 2010). The Cenozoic levels preserve sediments characteristic of fluvial, ephemeral lacustrine and aeolian environments associated in general with arid and semiarid climate conditions (Ciccioli et al., 2010), corresponding to the Puesto la Flecha (Caselli et al., 2002), Vallecito (Tripaldi, 2012), Vinchina (Turner, 1964), Zapallar (Furque, 1972) and El Corral Fms. (Furque, 1963). In the La Flecha range, the entire section has an approximate thickness of ~6 km.

Precise ages are unknown for the Ciénaga del Río Huaco, Puesto la Flecha, and Vallecito Fms. in the La Flecha and La Troya creeks (Fig. 1). For the top of the Ciénaga del Río Huaco Fm. (northern La Flecha range; Nacimientos) Tedesco et al. (2007) obtained a K–Ar age in a tuff of 108.1 ± 4.4 Ma. One hundred km to the south in the Huaco anticline section (Fig. 1), Fosdick et al. (2017) obtained detrital zircon U–Pb maximum depositional age (MDA) of 93.6 ± 7.3 Ma for the top of the same unit (~150 m thick), 36.8 ± 1.7 Ma for the Puesto la Flecha Fm. (~95 m thick) and between 32.6 ± 1.5 and 30.1 ± 0.5 Ma for the base of the Vallecito Fm. (~300 m thick). In the Valle Hermoso section (~122 Km to the north, see Fig. 1), Stevens Goddard and Carrapa (2018) obtained a MDA of 16.0 ± 0.3 Ma for the Vallecito Fm. (~300 m thick) based on U–Pb detrital zircons. In the same section, these authors propose for the Vinchina Fm. (~5500 m thick) MDA ages of 18.6 ± 0.4 Ma (U–Pb detrital zircons at the base of the unit), 13.8 ± 1.7 Ma (1000 m above the base), 9.2 ± 0.5 Ma. (at ~ 3220 m from the base) and 9.3 ± 0.4 Ma (top of the unit). Ciccioli et al. (2014) reported a MDA U–Pb age of 15.6 ± 0.4 Ma obtained from detrital zircons collected from a thick tuffaceous interval of the Lower Member of the Vinchina Fm. at La Cueva (Precordillera) and a depositional U–Pb age of 9.24 ± 0.034 Ma from a thin tuff bed in the Upper Member of this unit at Quebrada de Los Pozuelos (Northwestern Sierras Pampeanas). Within the La Flecha creek, Collo et al. (2015) published a MDA of 16.3 ± 1.2 Ma based on U–Pb analysis in detrital zircons of a tuff collected close to the base of the Vinchina Fm.

Farther to the north in the Vinchina section (see Fig. 1), Stevens Goddard and Carrapa (2018) document an age of 8.9 ± 2.5 Ma from the base of the overlying Toro Negro Fm. (~1400 m thick), correlated with the Zapallar Fm. in our study area. In the same section, U–Pb zircon ages from tuffs were used by Amidon et al. (2016) and Ciccioli et al. (2018) to propose depositional ages between ~ 6.9 ± 0.1 Ma at the base and 2.4 ± 0.03 Ma at the top of the Toro Negro Fm., and a MDA age <1.4 ± 0.5 Ma

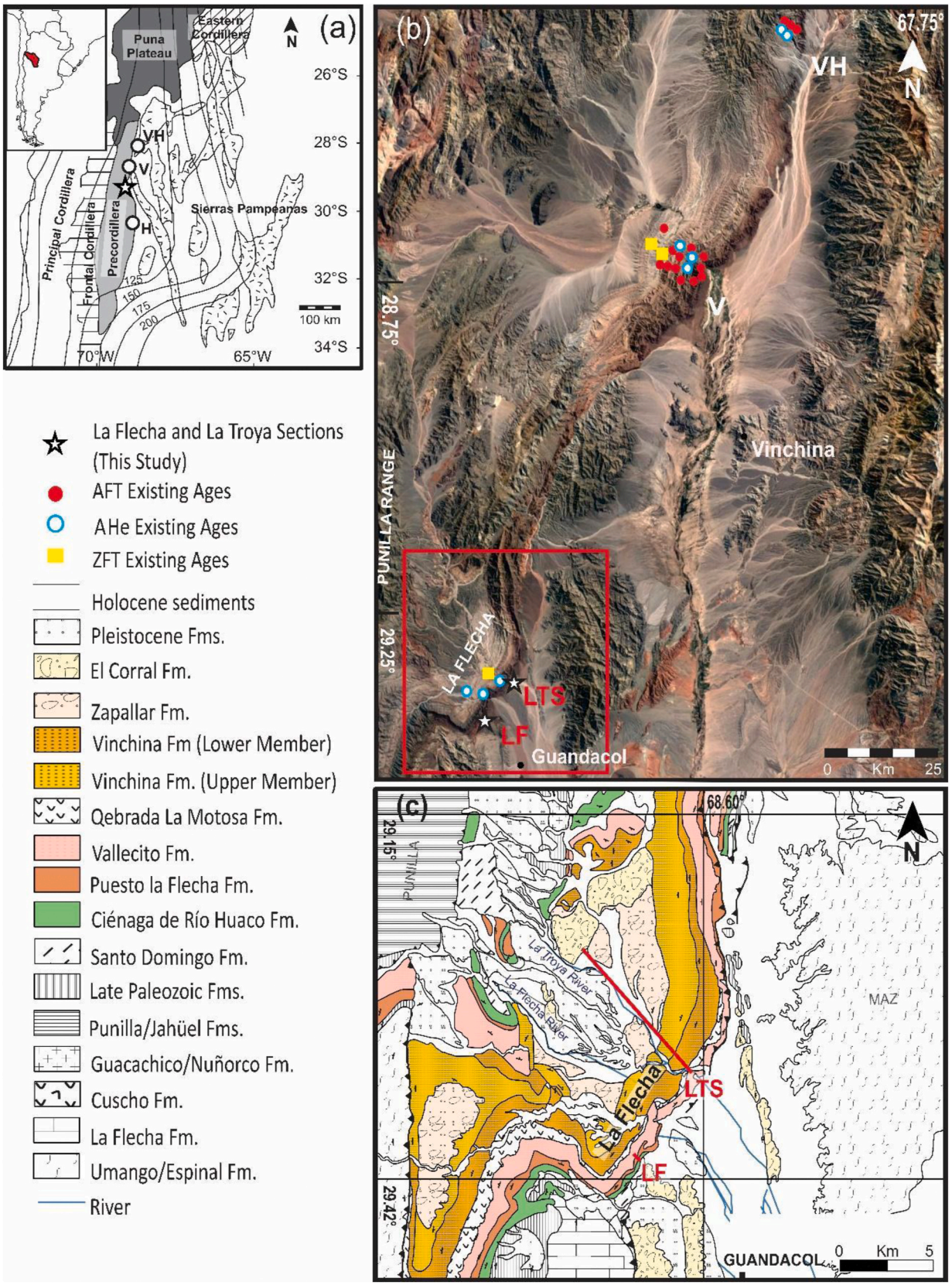

Fig. 1. **(a)** Tectonomorphic setting of the central Andes adapted from Stevens Goddard and Carrapa (2018). **(b)** Satellite image (Google Earth) with locations of published thermochronologic data (Tabbutt, 1986; Reynolds et al., 1990; Coughlin, 2000; Collo et al., 2015; Stevens Goddard and Carrapa, 2018). The study area is indicated with the red box. **(c)** Geological map of the La Troya-La Flecha depocenter (modified from Ciccioli et al., 2014). The study sections are also shown with red lines. VH: Valle Hermoso; V: Vinchina; H: Huaco; LF: La Flecha, HC: Huaco anticline, VN: Vinchina, VH: Valle Hermoso. AFT: Apatite Fission Track; AHe: Apatite (U–Th)/He; ZFT: Zircon Fission Track. LF: La Flecha section; LTS: La Troya section. (For interpretation of the references to color in this figure legend, the reader is referred to the Web version of this article.)

for the El Corral Fm., which discordantly lies immediately above the Toro Negro Fm.

Available thermochronological data of the Vinchina basin in the studied transect are scarce (Figs. 1 and 2). Stevens Goddard and Carrapa (2018) published single-grain AHe ages between 3.4 and 5.7 Ma for the base of the Vinchina Fm. and between 17 and 114.2 Ma for its middle part. For the same section, Collo et al. (2015) published single-grain AHe ages between 3.3 and 7.4 Ma for one sample at ~ 300 m from the base of the Vinchina Fm. In addition, Reynolds et al. (1990) published a central ZFT age tuff of 12.1 ± 2.8 Ma for the top of the Vinchina Fm. (Las Juntas section in their work). Location of complementary AFT and AHe data from the Vinchina and Valle Hermoso sections is shown in Fig. 1b.

3. Materials and methods

Twelve samples were taken from sandstones corresponding to Cretaceous-Cenozoic sedimentary units in the La Flecha and La Troya sections in order to perform AFT and (U–Th)/He analyzes. Apatite grains suitable for fission track dating and (U–Th)/He analyzes were concentrated and separated from their host rock samples by conventional mineral separation techniques. Overall, these minerals are naturally concentrated in sandstone and these kinds of rocks can be found throughout the entire studied section.

Each sample was stratigraphically located based on previous detailed studies (Caselli et al., 2002; Ciccioli et al., 2005; Collo et al., 2015). Sample location in the stratigraphic column and their coordinates are shown in Fig. 2 and Table 1, respectively.

3.1. Apatite (U–Th)/He analysis (AHe)

To carry out (U–Th)/He analyses, three to five apatite grains per sample were analyzed from four samples (TG011T, TG014T, TG016T and TG018T, see Fig. 2 and Table 1). Apatite concentration was performed at the Low Temperature Thermochronology Laboratory of the University of São Paulo. Each apatite grain was photographed and packed in 1 mm Pt tubes using an Olympus SZX16 stereoscopic microscope, following the procedure proposed by Farley (2002). The grain dimensions and the number of crystal terminations were determined to calculate the correction factor associated with alpha ejection (Ft, Farley et al., 1996). Helium measurements were performed at the University of Potsdam, Germany. The platinum tubes were loaded into a 25-hole sample chamber of an ASI Alphachron He analysis and extraction system, equipped with a 978 nm 30 W coherent diode laser and a Pfeiffer Prisma 200 Quadrupole mass spectrometer. The abundance of 4He in the purified gas was measured by isotope dilution using a 3He tracer, calibrated against a gauged 4He standard. A second analysis or re-extraction was performed for each sample to ensure that the grain was completely degassed. Following degassing, the analysis of U, Th and Sm was carried out at the GFZ Potsdam by isotope dilution using a Thermo Element 2 XR ICP-MS equipped with a CETAC ASX-520 automatic sampling system, and was run in the low resolution mode to maximize ion transmission. Age calculation followed the procedures of Meesters and Dunai (2005). An uncertainty of 2σ is reported for all ages. The potential effect of radiation damage on the AHe data was evaluated by comparing the effective uranium (e[U] = U + 0.235 * Th) and the grain size with individual ages (see Fig. 3) as a proxy for radiation damage, following the model by Flowers et al. (2009).

3.2. Apatite fission track analysis (AFT)

AFT analyzes were performed on 12 samples (see Fig. 2 and Table 1) following procedures described in Tagami and O'Sullivan (2005). The grinding and concentration of heavy minerals were carried out in the Heavy Minerals Grinding and Concentration laboratory of CICTERRA and in the Low Temperature Thermochronology Laboratory of the University of São Paulo. Two aliquots of each sample were prepared. One aliquot was analyzed for age determination by the External Detector Method (Gleadow and Duddy, 1981), using an Olympus BX51 microscope with a digitizing tablet and the FTStage 4.05 software (Dumitru, 1993) at the Low Temperature Thermochronology Laboratory of the São Paulo University. Ages and errors were calculated using the zeta calibration method (Hurford and Green, 1983), using a zeta calibration factor of 79.6 ± 1.8 (CN1 glass; Cecilia Wunderlin) obtained by analyzing a total of 9Durango and Fish Canyon Tuff age standards. An uncertainty of 1σ is reported for all ages. The other aliquot was irradiated with ^{252}Cf fission-fragments in order to make visible a greater number of confined tracks for length measurements (table SM2 in supplementary material). The AFT counting was performed on an average of 20 grains per sample (see Table 2 and table SM1 in supplementary material). The potential effects of variations in track annealing kinetics were evaluated by measuring Dpar values.

3.3. Multimethod thermochronological modeling

Multimethod inverse thermal modeling was applied in samples with AHe and AFT data. TG011T, TG014T, TG016T and TG018T samples were modeled using the QTQt v5.7.0 R software (Gallagher, 2012), considering all AHe aliquots and AFT ages (this is justified in section 4.4), track lengths and angles to the C-axis and using the Dpar measurements as a kinetic and compositional parameter. This allows probable thermal histories to be extracted using Bayesian transdimensional statistics. At least 500,000 interactions were performed. For the fission track annealing parameters, we used the kinetic model of Ketcham et al. (2007); for the AHe system, we used the radiation damage model of Flowers et al. (2009).

Taking into account the geological configuration of the modeled samples, we applied restrictions to the model based on geological information that includes the depositional age of each level (Table 1), an approximate exhumation age of the sections (~2 Ma according to Amidon et al., 2016) and the depositional (20 ± 5 °C) and current (20 ± 5 °C) temperatures. Maximum ages of ~200 Ma and maximum temperatures of 140 °C were used for the search space, considering that this is large enough not to influence the model.

3.4. 1D thermal modeling

Simplified reconstructions of the post-depositional and thermal history of the studied section were performed using the 1D-Petromod® software package. The main assumptions for modeling are: (1) because it is an entirely siliciclastic section, rock decompaction factors proposed by Sclater and Christie (1980) was used, (2) variations in seawater depth over time are assumed to be irrelevant, because all deposits involved in this study are continental and thermal evolution is mainly affected by sediment thickness rather than depth of the water; (3) a surface temperature of 20 °C is assumed and (4) variable heat flow values over time are assumed following the proposal of Collo et al. (2011). The 1D model was performed to obtain variations in heat flow values through time, allowing the maximum QTQt modeled temperatures to be reached. The thicknesses and ages of the stratigraphic units are shown in Table 1.

4. Results

4.1. AHe analyses

The results obtained for the four samples analyzed are shown in Table 2 and Fig. 2. Apatite grains had an equivalent spherical radius between 42.7 and 65.8 μm and eU contents between 2.9 and 70.8 ppm. AHe ages range from 5.7 ± 0.8 to 109.2 ± 2.2 and show an upsection increase in dispersion, so that some aliquots are older than the depositional ages and therefore represent partially reset ages (Figs. 2 and 4). The overall negative linear correlation between eU vs. AHe ages (Fig. 3) for most samples measured shows that the more commonly used models

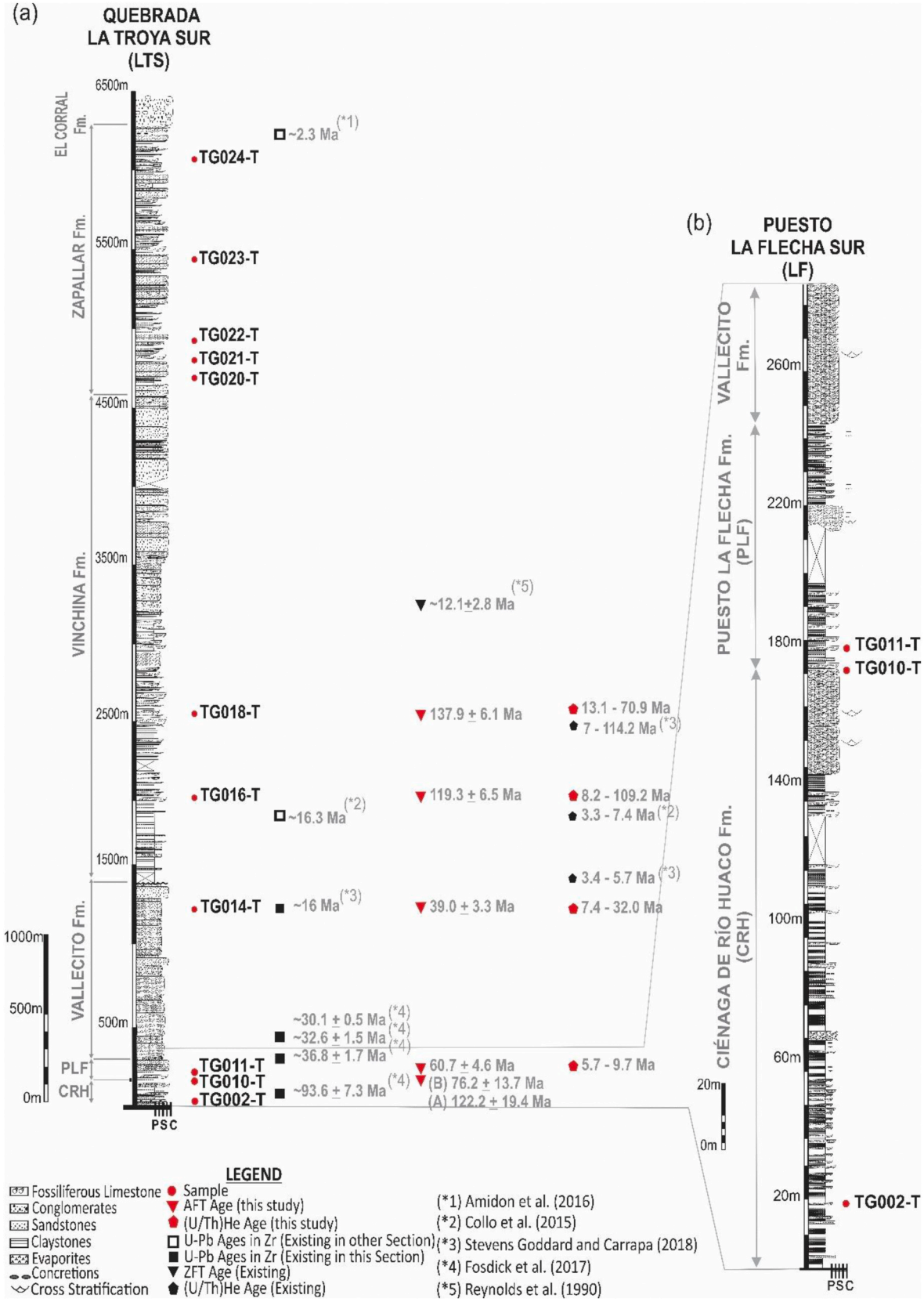

Fig. 2. **(a)** Stratigraphic columns of La Troya and La Flecha sections, modified from Caselli et al. (2002) and Collo et al. (2015). Sample positions, the respective AHe and AFT thermochronological ages, and UPb maximum depositional ages from this and previous works are indicated. Extrapolated depositional ages from other sections are shown with empty boxes. **(b)** Detailed stratigraphic column from La Flecha section.

Table 1
Sample location, depths (from the base of the El Corral Fm.) and U–Pb MDA (maximum depositional ages) for the studied units. (*1) Amidon et al. (2016), (*2) Collo et al. (2015), (*3) Stevens Goddard and Carrapa (20184iy), (*4) Fosdick et al. (2017). A detail of the analysis carried out in this work is shown in black circles. (*5) samples processed but not measured. NAG: samples without Apatite grains; AFT: Apatite Fission Track; AHe: Apatite (U–Th)/He; Cf: Californium irradiation.

Sample	Longitude (W)	Latitude (S)	Depth (m)	Stratigraphic section	Unit	Depositional age	U–Pb MDA (Ma)	Termocronological Ages		
								AHe	AFT	Cf
TG024T	68° 40′ 30.50"	29° 17′ 21.63"	~200	Qda. La Troya Sur	Zapallar Fm.	Upper Miocene	~2.3 (*1)		(*5)	
TG023T	68° 39′ 20.35"	29° 18′ 21.17"	~850			Upper Miocene (~10 Ma)			(*5)	
TG022T	68° 38′ 43.64"	29° 19′ 42.71"	~1350			Upper Miocene (~12 Ma)			(*5)	
TG021T	68° 38′ 36.28"	29° 19′ 43.48"	~1700			Upper Miocene	~6.9 (*1)		(*5)	
TG020T	68° 37′ 44.57"	29° 21′ 02.49"	~3350		Vinchina Fm.	Upper Miocene (~13 Ma)			(*5)	
TG018T	68° 37′ 18.12"	29° 21′ 22.04"	~3550			Upper-Mid Miocene (~15 Ma)		●	●	
TG016T	68° 37′ 05.35"	29° 21′ 19.15"	~4250			Upper-Mid Miocene	16.3 (*2)	●	●	●
TG014T	68° 36′ 17.75"	29° 21′ 30.82"	~5100	Puesto La Flecha Sur	Vallecito Fm.	Oligocene	16 (*3) 33 (*4)	●	●	●
TG011T	68° 40′ 11.30"	29° 25′ 39.09"	~6122		Puesto La Flecha Fm.	Eocene	~37 (*4)	●	●	●
TG010T A	68° 40′ 10.7940"	29° 25′ 39.68"	~6127			Eocene	~37 (*4)		●	
TG010T B	68° 40′ 10.79"	29° 25′ 39.68"	~6127			Eocene	~37 (*4)		●	
TG002T	68° 39′ 53.06"	29° 25′ 47.21"	~6280		Ciénaga de Río Huaco Fm.	Upper Cretaceous	~94 (*4)		NAG	●

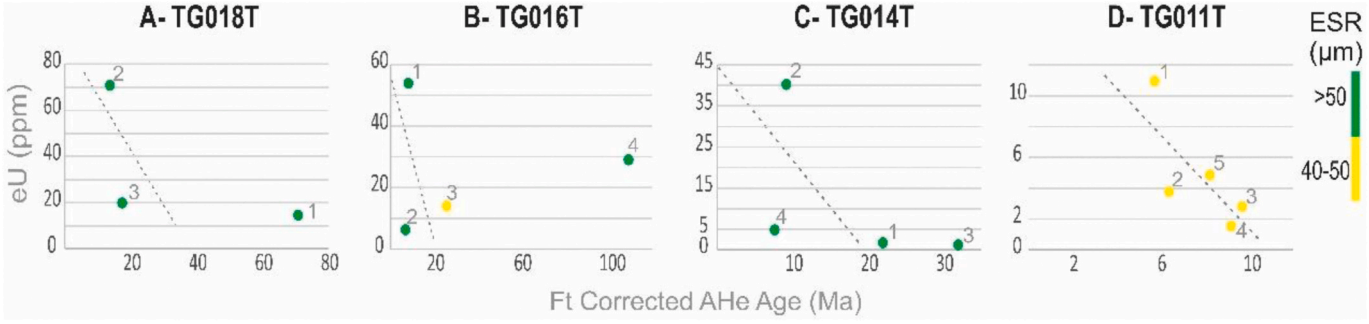

Fig. 3. eU (eU = U + 0.235Th) plotted versus Ft corrected AHe ages for single grains in samples TG018T, TG016T, TG014T, TG011T. The color of the marker indicates the grain size and the dotted lines delineate trends. The negative linear correlation between eU and AHe ages shows that radiation damage is not the main factor responsible for the age dispersion. (For interpretation of the references to color in this figure legend, the reader is referred to the Web version of this article.)

of radiation damage (Flowers et al., 2009; Gautheron et al., 2009), which predict enhanced He retentivity and hence older ages for damaged (i.e., eU-rich) grains, cannot explain the dispersion in AHe ages obtained (Fig. 3). It is likely that this dispersion is caused by samples with very different provenance histories and the effect of preservation of radiation damage from the source area. Therefore, used all aliquots for each sample in the model calculation. For the Puesto la Flecha Fm. (TG011T), five AHe ages between 5.7 and 9.7 Ma were obtained. These ages are younger than the depositional age of 37 Ma (Fig. 4), suggesting either total or partial resetting of the AHe system after sediment accumulation. For the Vallecito Fm. five AHe ages ranging between 7.4 and 32.0 Ma were acquired in sample TG014T. For the Vinchina Fm. four aliquots yield AHe ages between 8.2 and 109.2 Ma in sample TG016T, collected at 550 m from the base, and three aliquots from sample TG018T, collected at 1100 m above the base, yield ages between 13.1 and 70.9 Ma. Ages from all samples show a large dispersion, although for most of the samples, this is unrelated to variations in the effective uranium concentration (Fig. 3). As AHe ages from the Vinchina Fm. are older than the depositional ages (see Fig. 4), it is concluded that they were not reset during burial.

4.2. AFT analysis

The AFT central ages obtained are shown in Table 3 and Fig. 2. Mean track lengths (MTL) were obtained in 4 samples based on a variable amount of 4–99 confined tracks available (Table 2 and SM2 in Supplementary Material).

In the deepest sample, at the base of the Fm. Ciénaga de Río Huaco (TG002T), no apatite grains were identified. For the top of this unit (TG010T), AFT central ages of 122.2 ± 19.4 Ma and 76.2 ± 13.7 Ma were measured in two aliquots (A and B), respectively. TG010T-A is the only sample analyzed that passes the χ^2 test, but just 4 grains could be measured in it (see Table 3 and Fig. 5). About 10 m up section, at the base of the Puesto la Flecha Fm. (TG011T), an AFT central age of 60.7 ± 4.6 Ma (n = 18) and an MTL of 14.7 ± 1.4 μm (n = 4, Fig. 5d) were obtained. For the Vallecito Fm., sample TG014T yielded an AFT central age of 39.0 ± 3.3 Ma (n = 15) with a MTL of 11.3 ± 0.2 μm (n = 12, Fig. 5c). For the Vinchina Fm. two AFT central ages were obtained. A sample collected at 550 m from the base (TG016T) yielded an age of 119.3 ± 6.5 Ma (n = 24) and an MTL of 11.3 ± 0.3 μm (n = 43, Fig. 5b) and a sample at 1110 m from the base (TG018T) yielded an age of 137.9

Table 2
AHe analysis data.

Sample	Aliquot N°	FT corrected Age[a] (Ma)	1σ error Ma	Raw Age	U (ppm)	Th (ppm)	Sm (ppm)	Ue[b]	Th/U	He (nmol/g)	Mass (ug)	FT[c]	ESR[d] (μm)	Terminations
TG018T	1	70.9	0.7	56.4	7.6	30.0	44.2	14.6	4.1	4.6	4.83	0.80	65.8	0
	2	17.4	0.2	13.6	14.4	23.3	54.5	19.9	1.7	1.5	3.41	0.78	62.2	1
	3	13.1	0.1	10.0	46.0	105.7	27.5	70.8	2.4	3.8	3.91	0.77	59.8	0
TG016T	1	8.2	0.1	6.1	51.3	9.8	49.2	53.6	0.2	1.8	1.80	0.74	53.1	1
	2	6.9	0.2	5.3	4.3	7.6	109.4	6.1	1.8	0.2	3.03	0.76	60.2	1
	3	25.8	0.6	18.9	8.9	21.6	54.2	14.0	2.5	1.5	2.14	0.73	49.6	0
	4	109.2	1.1	81.1	19.0	42.5	70.3	29.0	2.3	13.1	3.17	0.74	59.2	1
TG014T	1	22.0	1.3	15.9	0.5	5.3	24.4	1.7	11.7	0.2	3.15	0.73	56.2	0
	3	9.4	0.1	6.9	21.5	79.7	39.2	40.2	3.8	1.5	2.99	0.73	58.1	1
	4	32.0	3.4	22.3	0.5	1.0	0.3	0.7	1.9	0.1	1.84	0.70	50.5	1
	5	7.4	0.4	5.5	2.4	10.2	25.0	4.8	4.3	0.2	2.67	0.75	53.4	0
TG011T	1	5.7	0.4	3.8	4.3	27.9	74.6	10.8	6.7	0.2	1.49	0.66	44.3	0
	2	6.5	0.9	4.4	2.3	6.2	16.7	3.8	2.8	0.1	1.38	0.68	42.7	0
	3	9.7	1.6	6.4	1.0	7.7	21.1	2.9	7.6	0.1	1.43	0.66	43.4	0
	4	9.2	1.3	6.3	0.8	3.4	9.4	1.6	4.5	0.1	1.78	0.68	47.3	0
	5	8.2	0.6	5.5	2.2	11.2	23.8	4.9	5.3	0.1	1.40	0.66	43.7	0

Notes.
[a] Age corrected using the grain geometry and ejection factor FT, error at 1σ.
[b] Effective uranium concentration.
[c] Geometric correction factor for age calculation.
[d] Equivalent spherical radius.

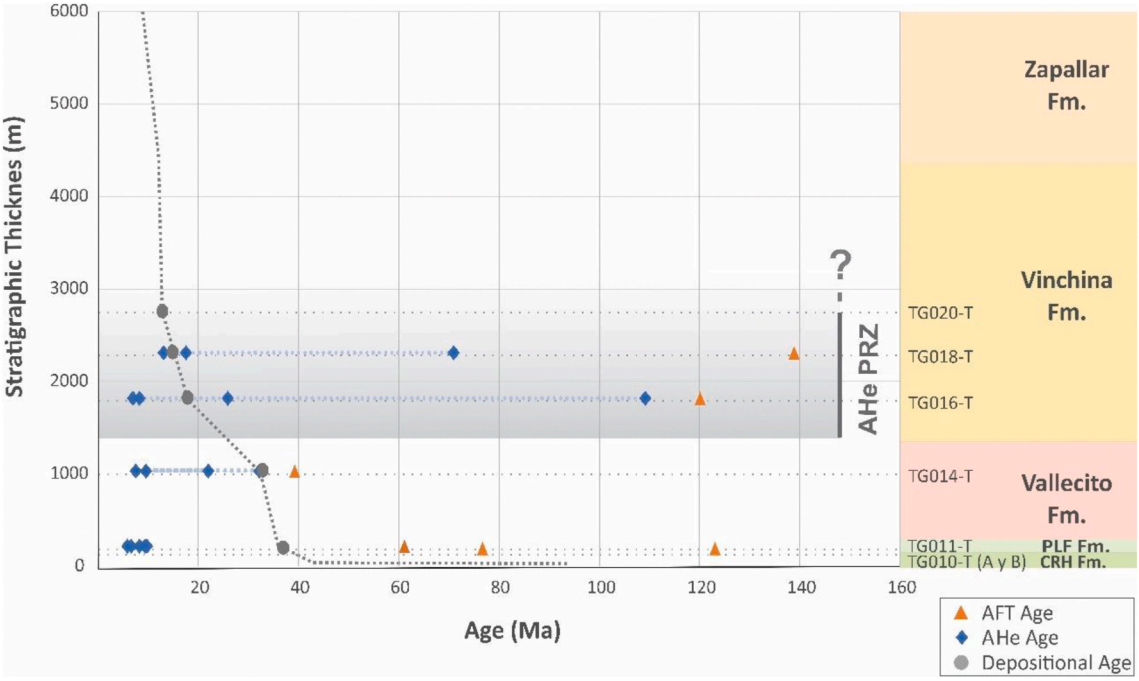

Fig. 4. Diagram of depositional ages vs. thermochronological ages (AFT central ages and single grain Ft-corrected AHe ages calculated for this study; Tables 2 and 3). AFT ages are older than depositional ages. AHe ages below TG014T are younger than depositional ages; however, above this sample, some aliquots are younger and some older than depositional ages.

± 6.1 Ma (n = 24) and a MTL of 13.6 ± 1.2 μm (n = 99, Fig. 5a).

A slightly bimodal track-length distribution (see Fig. 5), χ^2 test values < 5% (except sample TG010T-A) and the relationship between the obtained ages and the time of deposition (see Fig. 4) for all samples suggest that the AFT ages are unreset or, at most, partially reset.

Samples TG020T, TG021T, TG022T, TG023T and TG024T, collected stratigraphically up-section, were processed but, considering that all the samples analyzed at deepest levels do not show evidence of a complete resetting, were not analyzed (see Fig. 2 for location of the samples).

4.3. Multimethod thermochronological thermal modeling

The results of the multimethod QTQt modeling are shown in Fig. 6 and Table 4. In general, a decrease in the peak temperatures is observed upsection. In the deepest analyzed sample (TG011T, Puesto la Flecha Fm.) the modeled maximum temperatures are between 95 and 105 °C, showing partial reset AFT ages and total reset AHe ages (Figs. 4 and 7). Maximum temperatures gradually decrease to TG0014T (~95–105 °C) and TG016T (~90–100 °C) and, according to the model, these temperature peaks were reached in a time interval between 30 and 12 Ma (Table 4). The shallowest sample (middle section of the Vinchina Fm.)

Table 3
AFT analysis data. Zeta for WC analysis = 79.6 ± 1.8. Stratigraphical ages are approximated (see Fig. 2 form more details).

Sample	Stratigraphic Age (Ma)	N° of grains	Area (cm^2)	NS[a]	ND[b]	NI[c]	ρS[d] (cm^2)	ρD[e] (cm^2)	ρI[f] (cm^2)	Dpar (μm)	N° of Dpar	Age[g] (Ma)	±1σ Error	U (ppm)	P (χ^2)[h]	MTL[i] (μm)	Error (μm)	SD[j] (μm)	N° of length
TG018T	~15	26	1.26E-03	1642	16,308	1241	1.30 E+06	2.65 E+06	9.81 E+05	2.21	104	137.9	6.1	13.95	0	13.57	1.17	1.68	99
TG016T	~18	24	5.84E-04	909	16,308	791	1.56 E+06	2.63 E+06	1.36 E+06	2.24	96	119.3	6.5	19.37	0	11.27	0.30	1.92	43
TG014T	~16–33	15	5.39E-04	205	16,308	547	3.81 E+05	2.62 E+06	1.02 E+06	2.3	60	39.0	3.3	14.58	0	11.29	0.20	1.27	12
TG011T	~37	18	3.75E-04	314	16,308	534	8.38 E+05	2.61 E+06	1.42 E+06	1.91	72	60.7	4.6	20.56	0	14.67	1.44	2.87	4
TG010T A	~37	4	1.16E-04	89	16,308	74	7.69 E+05	2.58 E+06	6.39 E+05	3.08	16	122.2	19.4	9.32	0	–	–	–	–
TG010T B	~37	6	1.95E-04	55	16,308	74	2.82 E+05	2.59 E+06	3.79 E+05	2.69	24	76.2	13.7	5.51	98.9	–	–	–	–

Notes.
[a] Spontaneous track numbers.
[b] Number of induced tracks counted in the mica for estimating RhoD.
[c] Induced tracks number.
[d] Spontaneous tracks density.
[e] Induced track density measured in the external mica detector attached to CN1 dosimetry glass.
[f] Induced tracks density.
[g] Central (Pooled) age for samples passing (failing) the χ^2 test.
[h] Chi-square probability. Values greater than 5% are considered to pass this test and represent a single population of ages.
[i] Median confined track length measure.
[j] Standard deviation of measured lengths.

shows a maximum temperature of ~55 °C, which is consistent with a lack of resetting in the two systems analyzed (see Fig. 4). This temperature is achieved, according to the model, in a time interval between 15 and 1.5 Ma (Table 4).

The obtained models cannot reproduce all aliquots adequately, as some of them are only partially reset and the thermal history in the source area is most likely different for each aliquot. However, we decided to include them in the models because if the older aliquots are discarded, the models can overestimate the maximum temperatures reached by considering a total reset of the AHe system.

4.4. Petromod 1D thermal modeling

The results of the 1D Petromod thermal modeling (Fig. 7, Table 4, supplementary material SM3) shows that for the Ciénaga del Río Huaco, Puesto La Flecha and Vallecito Fms. the maximum temperatures obtained from thermochronological models (95 and 70 °C, respectively) would have been reached at ~15 Ma, with a sedimentary thickness of approx. 2750 m and a basal heat flux of 65 mW/m^2. After the temperature maximum was reached (from ~11 Ma) these units would have experienced cooling associated with a reduction of the basal heat flux to 20 mW/m^2, consistent with the AHe ages (between 5.3 and 9.6 Ma) obtained from the TG011T sample, despite the basin being in a subsidence stage. This cooling would be reinforced by a blanketing effect associated with an increment in the sedimentation rates during the deposition of the Vinchina Fm. (See Fig. 7). Furthermore, our 1D forward thermal model shows that the Vinchina and Zapallar Fms. experienced the entire heating and cooling history in a cooler regime, with peak temperatures (64 and 60 °C, respectively) reached at approximately 2 Ma, at the moment when the units would experience the maximum burial within the basin.

5. Discussion and concluding remarks

Thermochronological analysis together with 1D modeling allow inferring a complex relation between maximum temperatures and timing in the studied sections (Fig. 7 and Table 4). According to the models, the Ciénaga del Río Huaco, Puesto la Flecha and Vallecito Fms. would attain resetting temperatures for the AHe system (>80 °C) during the early Miocene, and they would have crossed the ~60 °C isotherm during the cooling trajectory between ~16 and 6 Ma. The Vinchina and Zapallar Fms. did not reach total resetting temperatures for the AHe system at any time during their burial. The thermal models (QTQt) show that the middle part of the Vinchina Fm. reached a maximum temperature of ~55 °C at ~5 Ma, that is, after the deposition of the part of the Cenozoic sediments. The deepest modeled sample (TG011T, Puesto La Flecha Fm.) would not have reached temperatures above the AFT closure temperature (>120 °C). Taken together, the data allows us to approximate the base of the Miocene PRZ for the AHe system (~80 °C, Farley, 2002) in this region to lie within the upper section of the Vallecito Fm. and the base of the Vinchina Fm. (Fig. 4).

Through the 1D Petromod thermal modeling we could associate the maximum temperatures reached, the burial and exhumation histories of the basin and the variations in heat flow that would have taken place in the region during the Miocene. Before ~15 Ma a thermal gradient of ~27 °C/km is estimated, while for the Pliocene we propose a geothermal gradient of <15 °C/km (both based on basal temperatures, sedimentary thicknesses and a surface temperature of 20 °C). The temporal gap between Miocene and Pliocene-Pleistocene maximum temperatures is interpreted as strongly associated with thermal flow variations (65 and 20 mW/m^2, respectively, see Fig. 7) likely associated with the installation of the flat slab subduction in the region (Gutscher et al., 2000; Collo et al., 2015), and also with the blanketing effect, and allow explaining the abrupt decrease in maximum temperatures modeled for the TG018T sample (~55 °C).

The complex time-temperature trajectory modeled in this work

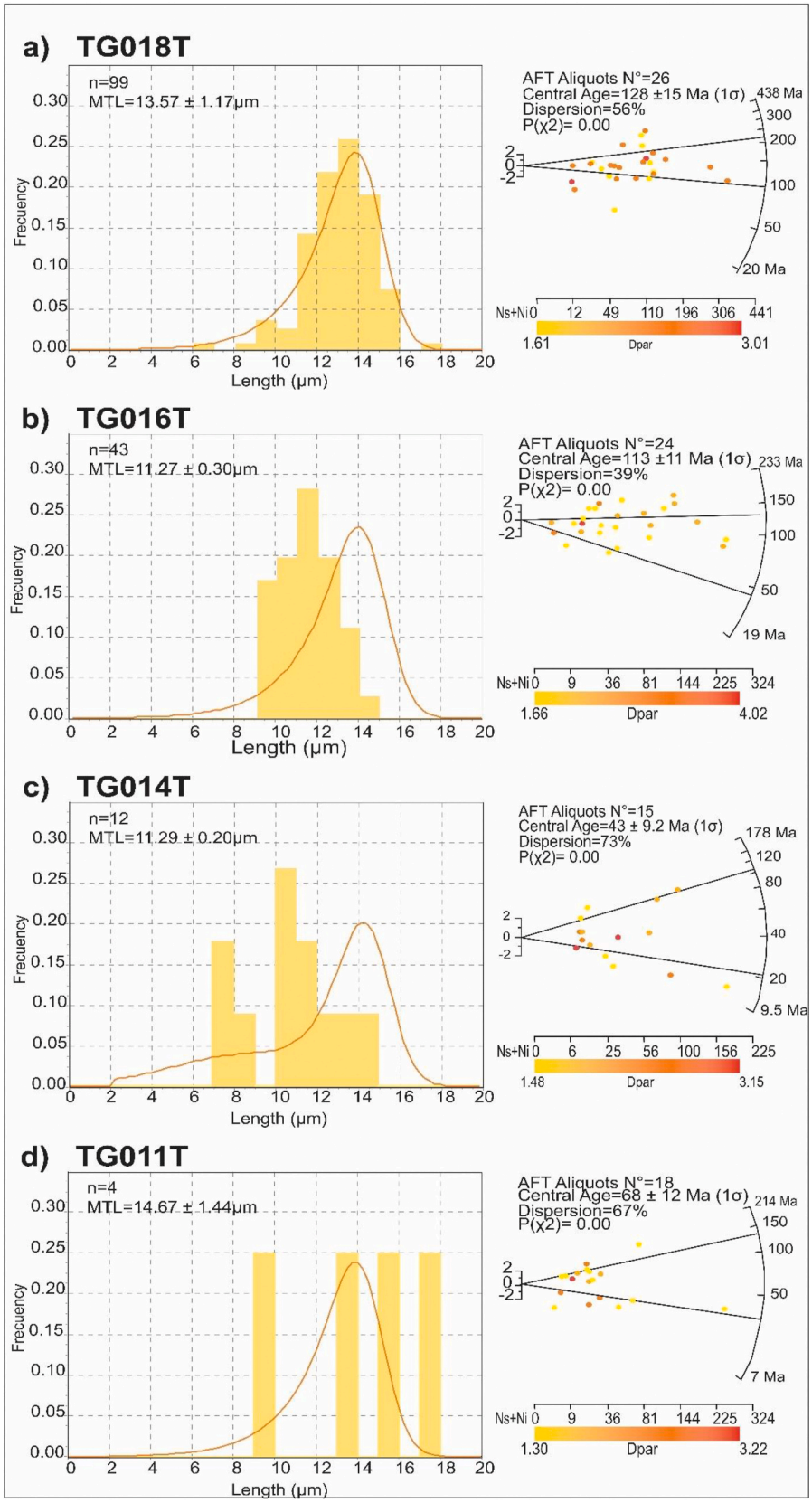

Fig. 5. Frequency histograms showing the distribution of track lengths and radial plots from AFT data in the four samples analyzed in this work (A-TG018T, B-TG016T, C-TG014T, D-TG011T). P(χ2): Chi-square probability. Values greater than 5% are considered to pass this test and represent a single population of ages. MTL: median confined track length.

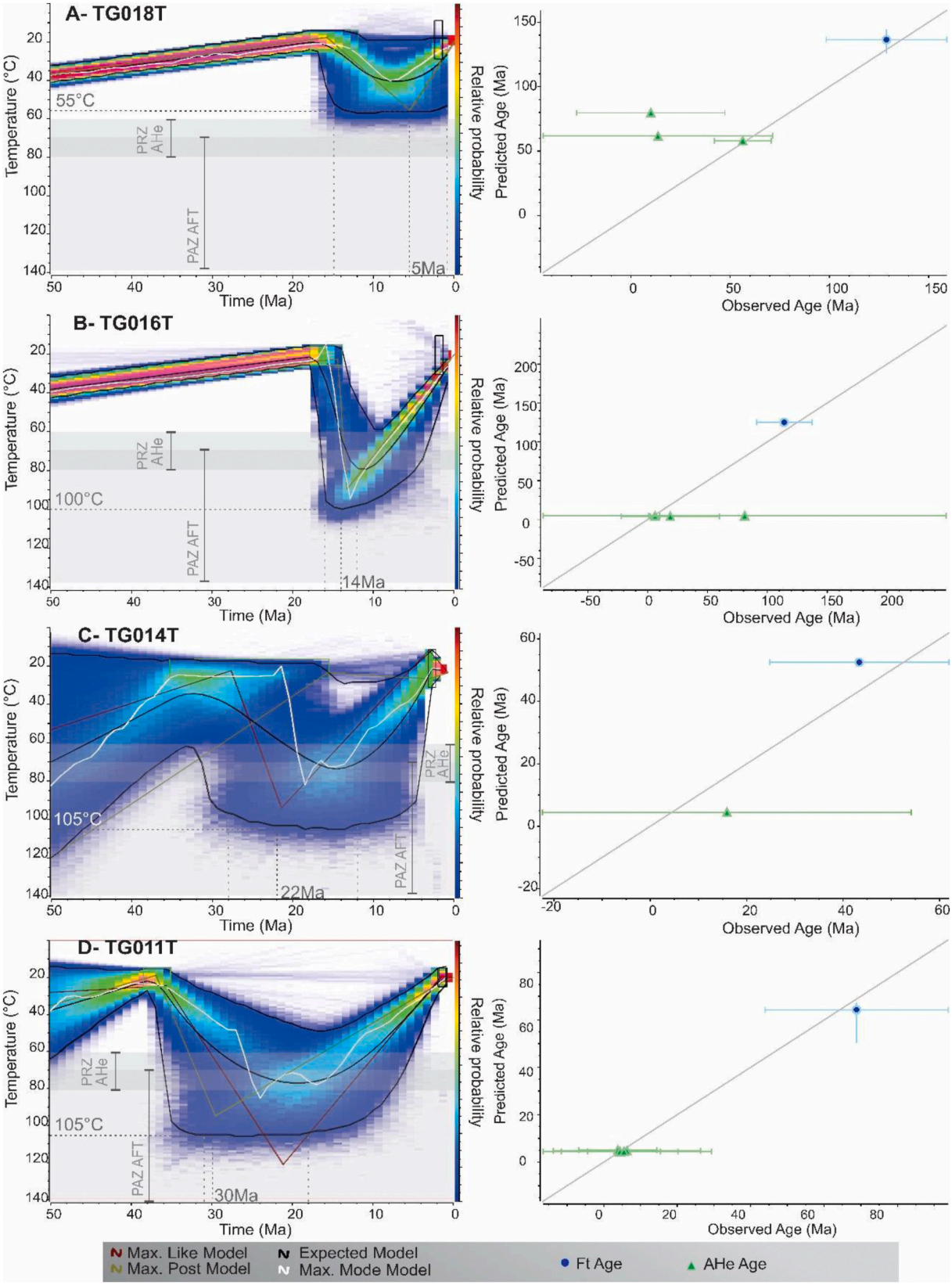

Fig. 6. QTQt multi-method inverse thermal modeling showing the t-T histories to the left and individual predictions (predicted ages vs. measured ages) to the right. The AHe and AFT results were modeled considering the depositional ages of each sample and the exhumation of the sections at ~2 Ma (Amidon et al., 2016). Light brown lines: maximum posterior models or best fit; red lines: maximum likelihood models; black lines: expected models; white lines: maximum mode models (further information can be found in Gallagher, 2012). Green triangles: AHe ages; blue circles: AFT ages. (For interpretation of the references to color in this figure legend, the reader is referred to the Web version of this article.)

Table 4
1D Thermal modeling data.

Sample	Depth (m)	QTQt Max. Temp.[a] (°C)	Time Interval[b] (Ma)	QTQt Best Fit Max[c] Temp. (°C)	Time[d] (Ma)	1D Modeling Max. Temp.[e] (°C)	Time interval[f] (Ma)
TG018T	−3950	55	1.5–15	55	5	60	2
TG016T	−4450	100	12–16	90	14	64	2
TG014T	−5300	105	12–28	95	22	70	15
TG011T	−6320	105	18–30	95	30	95	15

Notes.
[a] Maximum temperature reached by all tested t-T path in QtQt models.
[b] Time interval in which maximum temperatures are observed from all tested t-T path in QtQt models.
[c] Maximum temperature reached by best fit QtQt model. See Max. Like model line of Fig. 6.
[d] Time in which maximum temperatures for best fit are observed.
[e] Maximum temperature from 1D Petromod model.
[f] Time interval in which maximum temperatures are observed in 1D Petromod model.

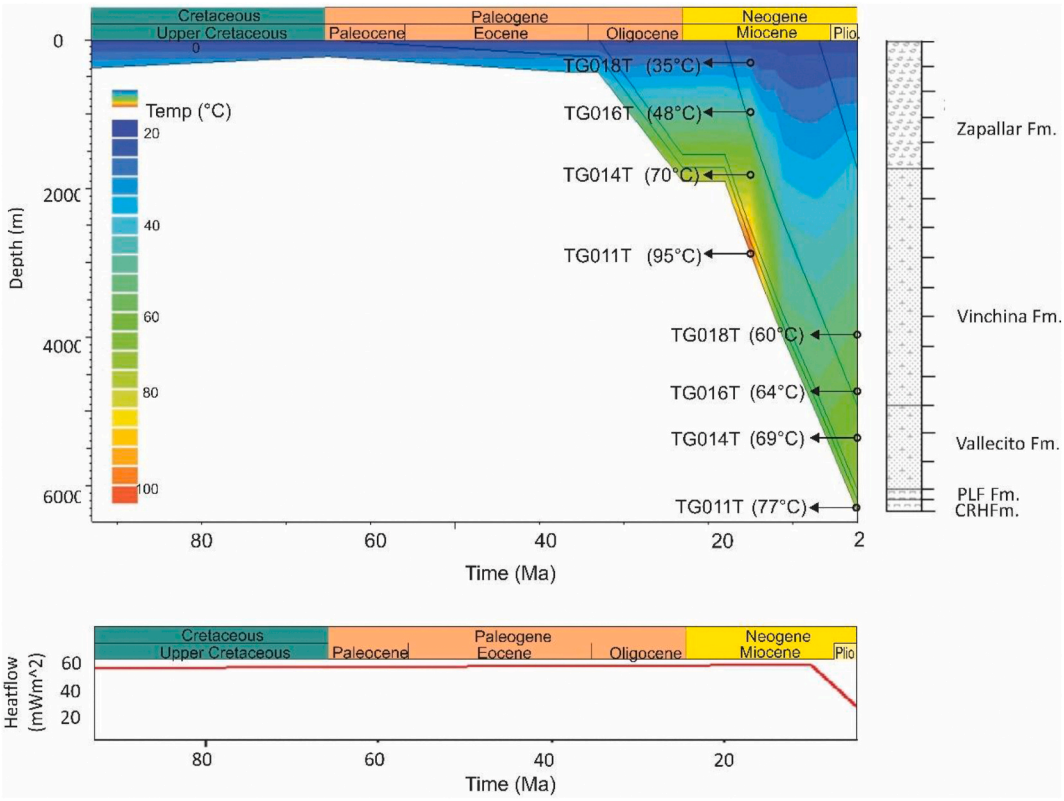

Fig. 7. a) 1D thermal modeling for the Cretaceous-Cenozoic units in the studied sections using PetroMod 1D Express software. A heat flux of 65 mW/m^2 until 15 Ma and a gradual decrease to 20 mW/m^2 from 11 Ma to the present are considered according to the model proposed by Collo et al. (2015) for the Vinchina basin. The model shows that maximum temperatures are reached at ~15 Ma for the Ciénaga del Río Huaco (CRHF), Puesto la Flecha (PLF) and Vallecito Formations and at ~2 Ma for the Vinchina and Zapallar Fms. Black circles show sample location. It can also be observed the blanketing effect from ~10 Ma and the recovery of a steady state for the last 5 My. **b)** Heat flux input conditions, (for more details see table SM3 in supplementary material).

reinforces the hypothesis of a change in heat flow during the installation of the flat slab and also support the thermal regime proposed by Collo et al. (2015) for the Vinchina basin based on AHe ages and clay minerals analysis, whose model considers a thermal flux of 65 mW/m^2 before to 15 Ma and a gradual decrease from that age to 20 mW/m^2 since 11 Ma to present. Likewise, these results are also consistent with the extremely low gradient in this foreland basin proposed by authors such as Dávila and Carter (2013), Richardson et al. (2013), Bense et al. (2014), Hoke et al. (2014) and Collo et al. (2018), as well as with those recorded for other flat slab regions (eg. Dumitru, 1990; Dumitru et al., 1991; Gutscher 2002; Manea and Manea 2011).

It should be noted, however, that the paleotemperature distribution in the studied sections is substantially different from that observed by Stevens Goddard and Carrapa (2018) for the Vinchina section, immediately to the north, which estimated Mio-Pliocene gradients of 25–35 °C/km. These authors record AFT ages which are interpreted as reset at approximately 5400 m from the surface of the Cenozoic section (middle section of the Vinchina Fm.; MDA: 9.2 ± 0.5 Ma; AFT age: 8.9 ± 3.5 Ma, Sample VN3-2020). Although track lengths for the analyzed samples are not available, the ages allow modeling and thus to discern whether they are completely or partially reset. The simple comparison between the ages obtained for levels with comparable maximum attained burial depths in our sections allows substantial differences to be corroborated. Sample VN3-4032 in the Vinchina section, located ~3400 m below from the base of the El Corral Fm., has an AFT age of 6.6 Ma (Stevens Goddard and Carrapa, 2018), while sample TG018T in the La Flecha section (this work), located ~ 3750 m below from the base of the El Corral Fm., yields an AFT age of 138.9 Ma and AHe ages between 13.1

and 70.9 Ma. Based on this comparison, it is likely that these substantial differences reflect local-regional variations in the thermal regime.

Lastly, it should be noted that the results obtained in this work allow us to sketch a complex thermal history for the Cretaceous-Cenozoic clastic successions in the La Flecha and La Troya Sur Sections, in which burial, exhumation and changes in the thermal regime are combined. The maximum time-temperature relationships records a cooling mechanism associated with the change in thermal flux, which does not correspond with the traditional concept in which the onset of cooling is directly related to the onset of exhumation and, at the same time, constitutes an advance in the understanding of the paleothermal regime of this particular Andean sector. Moreover, it is a solid baseline from which to move forward in future studies concerning the degree of preservation of primary thermal signals from clay minerals, fluid inclusions and isotopic analyses and define their reliability for paleoclimatic and paleoenvironmental interpretations.

Author statement

Cecilia Wunderlin: Conceptualization, Methodology, Formal analysis, Investigation, Resources, Writing - original draft, Visualization., Gilda Collo: Conceptualization, Validación, Resources, Writing - review & editing, Supervision, Project administration, Funding acquisition, Mauricio Parra: Methodology, Validación, Formal análisis, Investigation, Resources, Supervision, Project administration, Funding acquisition, Miguel Ezpeleta: Methodology, Validación, Resources, Writing - review & editing, Supervision, Project administration, Funding acquisition, Francisco Sánchez Nassif: Investigation, Writing - review & editing, Marlene Flores: Formal análisis, Investigation, Writing - review & editing., Edward R. Sobel: Validación, Investigation, Resources, Writing - review & editing. Johannes Glodny: Validación, Investigation, Resources, Writing - review & editing.

Declaration of competing interest

The authors declare that they have no known competing financial interests or personal relationships that could have appeared to influence the work reported in this paper.

Acknowledgments

We are grateful to the International Cooperation CONICET-FAPESP Project (2016, 23220160100035CO), the Agencia Nacional de Promoción Científica y Tecnológica (PICT 2017-3177), the Proyecto de Investigación UE 2016 - CONICET, for supporting our research work. Themochronometric analyses were funded by the FAPESP-CONICET SPRINT (Project 2016/50441-1). We are also grateful to CONICET for the PUE doctoral scholarship awarded to Cecilia Wunderlin. We would like to acknowledge the help of Graciela Toledo with the heavy minerals grinding and concentration in the CICTERRA, and to all the members of the Low Temperature Thermochronology Laboratory of the São Paulo University. We also thank the very constructive reviews and comments by two anonymous reviewers and the editorial recommendations that help improve this work.

Appendix A. Supplementary data

Supplementary data to this article can be found online at https://doi.org/10.1016/j.jsames.2020.102964.

References

Allmendinger, R.W., Judge, P.A., 2014. The Argentine Precordillera: a foreland thrust belt proximal to the subducted plate. Geosphere 10, 1203–1218. https://doi:10.1130/ges01062.1.

Amidon, W.H., Ciccioli, P.L., Marenssi, S.A., Limarino, C.O., Fisher, G.B., Burbank, D.W., Kylander-Clark, A., 2016. U-Pb ages of detrital and volcanic zircons of the Toro Negro Formation, northwestern Argentina: age, provenance and sedimentation rates. J. South Am. Earth Sci. 70, 237–250. https://doi.org/10.1016/j.jsames.2016.05.013.

Armstrong, P.A., 2005. Thermochronometers in sedimentary basins. Rev. Mineral. Geochem. 58, 499–525. https://doi.org/10.2138/rmg.2005.58.19.

Armstrong, P.A., Chapman, D.S., 1998. Beyond surface heat flow: an example from a tectonically active sedimentary basin. Geology 26, 183–186. https://doi.org/10.1130/0091-7613(1998)026<0183:BSHFAE>2.3.CO;2.

Bauluz, B., Yuste, A., Mayayo, M.J., Canudo, J.I., 2014. Early kaolinization of detrital weald facies in the galve sub-basin (central Iberian chain, north-east Spain) and its relationship to palaeoclimate. Cretac. Res. 50, 214–227. https://doi.org/10.1016/j.cretres.2014.03.014.

Bense, F.A., Wemmer, K., Löbens, S., Siegesmund, S., 2014. Fault gouge analyses: K-Ar illite dating, clay mineralogy and tectonic significance-a study from the Sierras Pampeanas, Argentina. Int. J. Earth Sci. 103, 189–218. https://doi.org/10.1007/s00531-013-0956-7.

Birks, H.H., Birks, H.J.B., 2006. Multi-proxy studies in palaeolimnology. Veg. Hist. Archaeobotany 15, 235–251. https://doi.org/10.1007/s00334-006-0066-6.

Caselli, A.T., Marenssi, S.A., Tripaldi, A., Limarino, C.O., Gagliardo, M., 2002. Análisis paleoambiental y correlación estratigráfica de la Formación Puesto La Flecha (Terciario), provincia de La Rioja. XV Congreso Geológico Argentino Actas I 679–683.

Ciccioli, P.L., Ballent, S., Tedesco, A.M., Barreda, V., Limarino, C.O., 2005. Hallazgo de depósitos cretácicos en la Precordillera de La Rioja (Formación Ciénaga del Río Huaco). Rev. la Asoc. Geol. Argentina 60, 122–131.

Ciccioli, P.L., Limarino, C.O., Marenssi, S.A., Tedesco, A.M., Tripaldi, A., 2010. Estratigrafía de la cuenca de Vinchina (Terciario), Sierras Pampeanas, provincia de La Rioja. Rev. la Asoc. Geol. Argentina 66, 146–155.

Ciccioli, P.L., Limarino, C.O., Friedman, R., Marenssi, S.A., 2014. New high precision U-Pb ages for the Vinchina formation: implications for the stratigraphy of the Bermejo andean foreland basin (La Rioja province, western Argentina). J. South Am. Earth Sci 56, 200–213. https://doi.org/10.1016/j.jsames.2014.09.005.

Ciccioli, P.L., Marenssi, S.A., Amidon, W.H., Limarino, C.O., Kylander-Clark, A., 2018. Alluvial to lacustrine sedimentation in an endorheic basin during the Mio-pliocene: the Toro Negro formation, central Andes of Argentina. J. South Am. Earth Sci. 84, 69–87. https://doi.org/10.1016/j.jsames.2018.03.011.

Clauer, N., Lerman, A., 2012. Thermal history analysis of sedimentary basins: an isotopic approach to Illitization. In: Analyzing the Thermal History of Sedimentary Basins: Methods and Case Studies. SEPM (Society for Sedimentary Geology), pp. 125–146. https://doi.org/10.2110/sepmsp.103.125.

Collo, G., Dávila, F.M., Nóbile, J., Astini, R.A., Gehrels, G., 2011. Clay mineralogy and thermal history of the Neogene Vinchina Basin, central Andes of Argentina: analysis of factors controlling the heating conditions. Tectonics 30, 1–18. https://doi.org/10.1029/2010TC002841.

Collo, G., Dávila, F.M., Teixeira, W., Nóbile, J.C., Sant′ Anna, L.G., Carter, A., 2015. Isotopic and thermochronologic evidence of extremely cold lithosphere associated with a slab flattening in the Central Andes of Argentina. Basin Res. 29, 16–40. https://doi.org/10.1111/bre.12163.

Collo, G., Ezpeleta, M., Dávila, F.M., Giménez, M., Soler, S., Martina, F., Ávila, P., Sánchez, F., Calegari, R., Lovecchio, J., Schiuma, M., 2018. basin thermal structure in the Chilean-pampean flat subduction zone. In: Folguera, A., Contreras-Reyes, E., Heredia, N., Encinas, A., Iannelli, S.B., Oliveros, V., Dávila, F.M., Collo, G., Giambiagi, L., Maksymowicz, A., Iglesia Llanos, M.P., Turienzo, M., Naipauer, M., Orts, D., Litvak, V.D., Alvarez, O., Arriagada, C. (Eds.), The Evolution of the Chilean-Argentinean Andes. United States of America, Springer, Cham, pp. 537–564. https://doi.org/10.1007/978-3-319-67774-3_21.

Coughlin, T.J., 2000. Linked Orogen-Oblique Fault Zones in the Central Argentine Andes: the Basis of a New Model for Andean Orogenesis and Metallogenesis. PhD thesis (Unpubished). University of Queensland, Queensland, p. 157.

Daoudi, L., Rocha, F., Ouajhain, B., Dinis, J.L., Chafiki, D., Callapez, P., 2008. Palaeoenvironmental significance of clay minerals in upper cenomanian–Turonian sediments of the western high atlas basin (Morocco). Clay Miner. 43, 615–630. https://doi.org/10.1180/claymin.2008.043.4.07.

Daoudi, L., Ouajhain, B., Rocha, F., Rhouta, B., Fagel, N., Chafiki, D., 2010. Comparative influence of burial depth on the clay mineral assemblage of the Agadir-Essaouira basin (western High Atlas, Morocco). Clay Miner. 45, 453–467. https://doi.org/10.1180/claymin.2010.045.4.453.

Dávila, F.M., Carter, A., 2013. Exhumation history of the andean broken foreland revisited. Geology 41, 443–446. https://doi.org/10.1130/G33960.1.

Dumitru, T.A., 1990. Subnormal Cenozoic geothermal gradients in the extinct Sierra Nevada magmatic arc: consequences of Laramide and Post-Laramide shallow-angle subduction. J. Geophys. Res. 95, 4925–4941. https://doi.org/10.1029/JB095iB04p04925.

Dumitru, T.A., 1993. A new computer-automated microscope stage system for fission-track analysis. Int. J. Radiat. Appl. Instrumentation. Part 21, 575–580. https://doi.org/10.1016/1359-0189(93)90198-I.

Dumitru, T.A., Gans, P.B., Foster, D.A., Miller, E.L., 1991. Refrigeration of the western Cordilleran lithosphere during Laramide shallow-angle subduction. Geology 19, 1145–1148. https://doi.org/10.1130/00917613(1991)019<1145:ROTWCL>2.3.CO;2.

Fagel, N., 2007. Chapter four clay minerals, deep circulation and climate. Dev. Mar. Geol. 1, 139–184. https://doi.org/10.1016/S1572-5480(07)01009-3.

Farley, K.A., 2002. U-Th)/He dating: techniques, calibrations, and applications. Rev. Mineral. Geochem. 47, 819–844. https://doi.org/10.2138/rmg.2002.47.18.

Farley, K.A., Wolf, R.A., Silver, L.T., 1996. The effects of long alpha-stopping distances on (U-Th)/He ages. Geochem. Cosmochim. Acta 60, 4223–4229. https://doi.org/10.1016/S0016-7037(96)00193-7.

Flowers, R.M., Ketcham, R.A., Shuster, D.L., Farley, K.A., 2009. Apatite (U-Th)/He thermochronometry using a radiation damage accumulation and annealing model. Geochem. Cosmochim. Acta 73, 2347–2365. https://doi.org/10.1016/j.gca.2009.01.015.

Fosdick, J.C., Reat, E.J., Carrapa, B., Ortiz, G., Alvarado, P.M., 2017. Retroarc basin reorganization and aridification during Paleogene uplift of the southern central Andes. Tectonics 36, 493–514. https://doi.org/10.1002/2016TC004400.

Franzese, J.R., Spalletti, L.A., Gómez Pérez, I., MacDonald, D., 2003. Tectonic and palaeoenvironmental evolution of Mesozoic sedimentary basins along the Andean foothills of Argentina (32° - 54° S). J. South Am. Earth Sci. 16, 81–90.

Descripción Geológica de la Hoja 17b Furque, G., 1963. Guandacol (Provincias de La Rioja y San Juan), vol. 92. Dirección Nacional de Geología y Minería, Boletín, Buenos Aires, p. 104.

Descripción geológica de la Hoja 16b Furque, G., 1972. Cerro La Bolsa, provincias de La Rioja y San Juan, vol. 125. Dirección Nacional de Geología y Minería, Boletín, Buenos Aires, p. 69.

Gallagher, K., 2012. Transdimensional inverse thermal history modeling for quantitative thermochronology. J. Geophys. Res. Solid Earth 117, 1–16. https://doi.org/10.1029/2011JB008825.

Gans, C.R., Beck, S.L., Zandt, G., Gilbert, H., Alvarado, P., Anderson, M., Linkimer, L., 2011. Continental and oceanic crustal structure of the Pampean flat slab region, western Argentina, using receiver function analysis: new high-resolution results. Geophys. J. Int. 186, 45–58. https://doi.org/10.1111/j.1365-246X.2011.05023.x.

Gautheron, C., Tassan-Got, L., Barbarand, J., Pagel, M., 2009. Effect of alpha-damage annealing on apatite (U-Th)/He thermochronology. Chem. Geol. 266, 166–179. https://doi.org/10.1016/j.chemgeo.2009.06.001.

Gleadow, A.J.W., Duddy, I.R., 1981. A natural long-term track annealing experiment for apatite. Nucl. Tracks 5, 169–174. https://doi.org/10.1016/0191-278X(81)90039-1.

Gutscher, M.A., 2002. Andean subduction styles and their effect on thermal structure and interplate coupling. J. South Am. Earth Sci. 15, 3–10.

Gutscher, M.A., Spakman, W., Bijwaard, H., Engdahl, E.R., 2000. Geodynamics of flat subduction: seismicity and tomographic constraints from the Andean margin. Tectonics 19, 814–833. https://doi.org/10.1029/1999TC001152.

Hoke, G.D., Giambiagi, L.B., Garzione, C.N., Mahoney, J.B., Strecker, M.R., 2014. Neogene paleoelevation of intermontane basins in a narrow, compressional mountain range, southern Central Andes of Argentina. Earth Planet Sci. Lett. 406, 153–164. https://doi.org/10.1016/j.epsl.2014.08.032.

Hower, J., Eslinger, E.V., Hower, M.E., Perry, E.A., 1976. Mechanism of burial metamorphism of argillaceos sediment. Geol. Soc. Am. Bull. 87, 725–737. https://doi.org/10.1130/0016-7606(1976)87<725.

Hurford, A.J., Green, P.F., 1983. The zeta age calibration of fission-track dating. Isot. Geosci. 1, 285–317.

Jordan, T.E., Allmendinger, R.W., Damanti, J.F., Drake, R.E., 1993. Chronology of motion in a complete thrust belt: the Precordillera, 30-31°S, Andes Mountains. J. Geol. 101, 135–156. https://doi.org/10.1086/648213.

Jordan, T.E., Schlunegger, F., Cardozo, N., 2001. Unsteady and spatially variable evolution of the Neogene Andean Bermejo foreland basin, Argentina. J. South Am. Earth Sci. 14, 775–798. https://doi.org/10.1016/S0895-9811(01)00072-4.

Kay, S.M., Mpodozis, C., 2002. Magmatism as a probe to the Neogene shallowing of the Nazca plate beneath the modern Chilean flat-slabs. J. South Am. Earth Sci. 15, 39–57. https://doi.org/10.1016/S0895-9811(02)00005-6.

Kay, S.M., Mpodozis, C., Ramos, V.A., Munizaga, F., 1991. Magma source variations for mid-late Tertiary magmatic rocks associated with a shallowing subduction zone and a thickening crust in the central Andes (28 to 33 ° S). Spec. Pap. Geol. Soc. Am. 265, 113–137.

Ketcham, R.A., 2012. basin thermal history analysis using (U-Th)/He thermochronometry. Anal. Therm. Hist. Sediment. Basins Methods Case Stud. 105–123 https://doi.org/10.2110/sepmsp.103.105.

Ketcham, R.A., Donelick, R.A., Carlson, W.D., 1999. Variability of apatite fission-track annealing kinetics: II. Crystallographic orientation effects. Am. Mineral. 84, 1224–1234. https://doi.org/10.2138/am-1999-0902.

Ketcham, R.A., Carter, A., Donelick, R.A., Barbarand, J., Hurford, A.J., 2007. Improved modeling of fission-track annealing in apatite. Am. Mineral. 92, 799–810. https://doi.org/10.2138/am.2007.2281.

Limarino, C.O., Net, L., Gutierrez, P., Barreda, V., Caselli, A., Ballent, S., 2000. Lithostratigraphical definition of the Cienaga del Rio Huaco Formation (Cretaceous), Precordillera central, San Juan, Argentina. Rev. la Asoc. Geol. Argentina 55, 83–89.

Limarino, C.O., Tripaldi, A., Marenssi, S.A., Net, L., Re, G., Caselli, A., 2001. Tectonic control on the evolution of the fluvial systems of the Vinchina Formation (Miocene), northwestern Argentina. J. South Am. Earth Sci. 14, 751–762. https://doi.org/10.1016/S0895-9811(01)00067-0.

Mahoney, L., McLaren, S., Hill, K., Kohn, B., Gallagher, K., Norvick, M., 2019. Late Cretaceous to Oligocene burial and collision in western Papua New Guinea: Indications from low-temperature thermochronology and thermal modelling. Tectonophysics 752, 81–112. https://doi.org/10.1016/j.tecto.2018.12.017.

Manea, V.C., Manea, M., 2011. Flat-slab thermal structure and evolution beneath central Mexico. Pure Appl. Geophys. 168, 1475–1487.

Meesters, A.G.C.A., Dunai, T.J., 2005. A noniterative solution of the (U-Th)/He age equation. G-cubed 6, 1–3. https://doi.org/10.1029/2004GC000834.

Merriman, R.J., Peacor, D.R., 1999. Very low-grade metapelites: mineralogy, microfabrics and measuring reaction progress. In: Frey, M., Robinson, D. (Eds.), Low-Grade Metamorphism. Blackwell Sci., Oxford, U. K.

Naeser, N.D., Naeser, C.W., McCulloh, T.H., 1989. The application of fission-track dating to the depositional and thermal history of rocks in sedimentary basins. In: Naeser, N. D., McCulloh, T.H. (Eds.), Thermal History of Sedimentary Basins. Springer, New York, N. Y. https://doi.org/10.1007/978-1-4612-3492-0_10.

Net, L.I., Alonso, M.S., Limarino, C.O., 2002. Source rock and environmental control on clay mineral associations, lower section of paganzo group (carboniferous), northwest Argentina. Sediment. Geol. 152, 183–199. https://doi.org/10.1016/S0037-0738(02)00068-4.

Pujols, E.J., Stockli, D.F., Constenius, K.N., Horton, B.K., 2020. Thermochronological and geochronological constraints on Late Cretaceous unroofing and proximal sedimentation in the Sevier orogenic belt, Utah. Tectonics 39, e2019TC005794. https://doi.org/10.1029/2019TC005794.

Ramos, V.A., Folguera, A., 2009. Andean flat-slab subduction through time. Geol. Soc. Spec. Publ. 327, 31–54. https://doi.org/10.1144/SP327.3.

Ramos, V.A., Cristallini, E.O., Pérez, D.J., 2002. The pampean flat-slab of the central Andes. J. South Am. Earth Sci. 15, 59–78. https://doi.org/10.1016/S0895-9811(02)00006-8.

Raucsik, B., Varga, A., 2008. Climato-environmental controls on clay mineralogy of the Hettangian-Bajocian successions of the Mecsek Mountains, Hungary: an evidence for extreme continental weathering during the early Toarcian oceanic anoxic event. Palaeogeogr. Palaeoclimatol. Palaeoecol. 265, 1–13. https://doi.org/10.1016/j.palaeo.2008.02.004.

Reynolds, J.H., Jordan, T.E., Johnson, N.M., Damanti, J.F., Tabbutt, K.D., 1990. Neogene deformation of the flat-subduction segment of the Argentine- Chilean Andes: magnetostratigraphic constraints from Las Juntas, La Rioja province, Argentina. Geol. Soc. Am. Bull. 102, 1607–1622. https://doi.org/10.1130/0016-7606(1990)102<1607:NDOTFS>2.3.CO;2.

Richardson, T., Ridgway, K.D., Gilbert, H., Martino, R., Enkelmann, E., Anderson, M., Alvarado, P., 2013. Neogene and Quaternary tectonics of the Eastern Sierras Pampeanas, Argentina: active intraplate deformation inboard of flat-slab subduction. Tectonics 32, 780–796. https://doi.org/10.1002/tect.20054.

Ruffell, A., McKinley, J.M., Worden, R.H., 2002. Comparison of clay mineral stratigraphy to other proxy paleoclimate indicators in the Mesozoic of NW Europe. Philos. Trans. R. Soc. A Math. Phys. Eng. Sci. 360, 675–693. https://doi.org/10.1098/rsta.2001.0961.

Sclater, J.G., Christie, P.A.F., 1980. Continental stretching: an explanation of the post-mid-cretaceous subsidence of the central north sea basin. J. Geophys. Res. Solid Earth 85, 3711–3739. https://doi.org/10.1029/jb085ib07p03711.

Stevens Goddard, A.L., Carrapa, B., 2018. Using basin thermal history to evaluate the role of Miocene–Pliocene flat-slab subduction in the southern Central Andes (27° S–30° S). Basin Res. 30, 564–585. https://doi.org/10.1111/bre.12265.

Tabbutt, K.D., 1986. Fission track chronology of foreland basins. PhD. thesis. In: The Eastern Andes: Magmatic and Tectonic Implications. Dartmouth College.

Tagami, T., O'Sullivan, P.B., 2005. Fundamentals of fission-track thermochronology. Rev. Mineral. Geochem. 58, 19–47. https://doi.org/10.2138/rmg.2005.58.2.

Tedesco, A.M., Limarino, C.O., Ciccioli, P.L., 2007. Primera edad radimétrica de los depósitos cretácicos de la Precordillera Central. Rev. Asoc. Geol. Arg. 62, 471–474.

Thiry, M., 2000. Palaeoclimatic interpretation of clay minerals in marine deposits: an outlook from the continental origin. Earth Sci. Rev. 49, 201–221. https://doi.org/10.1016/S0012-8252(99)00054-9.

Thiry, M., Dupuis, C., 2000. Use of clay minerals for paleoclimatic reconstructions: limits of the method with special reference to the Paleocene-lower Eocene interval. GFF 122, 166–167. https://doi.org/10.1080/11035890001221166.

Tripaldi, A., 2012. La Formación Vallecito como ejemplo de sedimentación eólica cenozoica de las cuencas andinas del Noroeste Argentino: paleoambientes y consideraciones estratigráficas y paleoclimáticas. An. Acad. Nac. Ciencias Exactas, Físicas y Nat. 64, 55–71.

Turner, J.C.M., 1964. Descripción geológica de la Hoja 15c. Vinchina (Provincia de La Rioja). Dirección Nacional de Geología y Minería. Boletín 100, Buenos Aires, p. 81p.

Yañez, G.A., Cembrano, J., Pardo, M., Ranero, C., Selles, D., 2002. The Challenger Juan Fernández Maipo major tectonic transition of the Nazca Andean subduction system at 3334VS: geodynamic evidence and implications. J. South Am. Earth Sci. 15, 23–38.